Microscopic nature of the charge-density wave in kagome superconductor RbV_3Sb_5 - Supplemental Material

Jonathan Frassineti,[1] Pietro Bonfà,[2] Giuseppe Allodi,[2] Roberto De Renzi,[2] Erick Garcia,[3] Rong Cong,[3] Brenden R. Ortiz,[4] Stephen D. Wilson,[4] Vesna F. Mitrović,[3] and Samuele Sanna[1]

[1] *Dipartimento di Fisica e Astronomia "A. Righi", Universitá di Bologna, I-40127 Bologna, Italy*

[2] *Dipartimento di Scienze Matematiche, Fisiche e Informatiche, Universitá di Parma, I-43124 Parma, Italy*

[3] *Department of Physics, Brown University, Providence, Rhode Island 02912, USA*

[4] *Materials Department and California Nanosystems Institute, University of California Santa Barbara, Santa Barbara, California 93106, USA*

I. METHODS

Sample preparation. Single crystals of RbV_3Sb_5 were grown from Rb ingot (purity 99.75 %), V powder (purity 99.9 %) and Sb grains (purity 99.999 %) using the self-flux method[1,2]. All the information regarding the procedure can be found in the above references. The obtained crystals have a typical size of $2 \times 2 \times 0.02$ mm^3. RbV_3Sb_5 single crystals are stable in the air.

NMR/NQR methods. Temperature dependent ^{51}V and ^{87}Rb nuclear magnetic resonance (NMR) and ^{121}Sb zero-field nuclear quadrupolar resonance (NQR) experiments were performed at the University of Parma (Italy) in an external magnetic field of 7.95 T (when applied) by means of a home-built broadband phase-coherent NMR spectrometer[3] and a nitrogen-flow cryostat or in liquid nitrogen bath; and at Brown University (USA), with a commercial NMR spectrometer and a helium-flow cryostat in a magnetic field of 6.99 T. The ^{121}Sb NQR spectrum at 77.3 K (Fig. 2b of the main paper) was measured by immersing the tuned LC probe head directly in liquid nitrogen inside a nitrogen dewar, which provided a hold time of several days with excellent sample temperature stability and allowed recording spin echo signals at high averaging statistics ($\approx 5 \times 10^5$ scans), as needed to detect the weaker and broader Sb1 peaks with a good signal-to-noise ratio. Spin echoes were excited at discrete frequencies with typical frequency stepping of 50 or 100 kHz, by employing either a standard equal-pulse spin echo sequence $P - \tau - P - \tau - echo$ or a three-pulse stimulated spin echo sequence $\pi/2 - \tau - \pi/2 - \tau' - \pi/2 - \tau - echo$[4,5], with suitable phase alternation of pulses and delays τ just longer than the receiver dead time but, in all cases, well shorter than the spin-spin relaxation time T_2. In the former, the two rf pulses P were

optimized for maximum signal intensity (a condition corresponding to a nutation angle of $4\pi/3$[4]). The stimulated echo sequence was mostly employed to detect the weaker ^{121}Sb NQR, in spite of its slightly reduced refocusing efficiency, owing to its immunity to spurious magneto-acoustic (ringing) and magneto-elastic couplings which, on the contrary, may affect the basic two-pulse excitation sequence by yielding spurious echo signals which are not completely rejected by phase cycling. In either case, spectra were reconstructed as the envelope of the frequency-shifted, phase-corrected Fourier transforms of the various spin echoes recorded at different reference frequencies. Such a method can be regarded as a variant of the frequency step and sum method illustrated in Ref. 6, more suited than the latter to the analysis of frequency-swept spectra.

Ab initio calculations. The electric field gradient (EFG) tensors at all nuclear sites have been predicted with the density functional theory-based code Elk[7]. The code uses the augmented plane wave basis plus local orbitals (APW+l.o.) to describe both core and valence electrons on the same footing. In order to accurately characterize the charge distribution close to the nucleus, the angular expansion of the inner part of the muffin tin has been set to $l = 4$. The remaining basis-related parameters were set by the "highq" setting. Spin-orbit coupling was also considered in all simulations.

A Methfessel-Paxton (order 1, see Ref. 8) electronic smearing of 100 meV was chosen to improve convergence. The Perdew, Burke, and Ernzerhof (PBE) exchange and correlation functional[9] was used and a 6x6x6 Monkhorst-Pack k-point set[10,11] was used to sample the reciprocal space.

The atomic positions reported in Ref. [12] for the pristine, the Star of David (SD), and the Inverse Star of David (ISD) structures were chosen. In good agreement with previous results, we found that the ISD structure has the lowest energy and $E_{SD} - E_{ISD} = 29.5$ meV/cell (36 atoms).

Owing to the presence of systematic errors in the absolute values of the computed EFGs, in the main paper we do compare the shift in ν_Q obtained from the changes in the EFG tensors of the pristine, ISD, and SD structures, namely $\Delta\nu_Q$, across the CDW transition. The comparison between DFT and experimental results of the absolute values of the quadrupolar frequency ν_Q in the pristine phase ($T > T_{CDW}$) is shown in Tab. I.

	Experiment (T = 200 K)				DFT (Kagome unit-cell)			
Atom	Rb	Sb1	Sb2	V	Rb	Sb1	Sb2	V
ν_Q (MHz)	1.7336	70.7125	72.1960	0.7034	1.8215	62.9870	65.4803	0.5976
η	0	0	0	-	0	0	0	0.416

TABLE I: Comparison of experimental and calculated parameters of the nuclear quadrupolar frequency $\Delta\nu_Q$ in the pristine phase of RbV_3Sb_5. Missing experimental values are reported with a dash.

II. SUPPLEMENTARY FIGURES

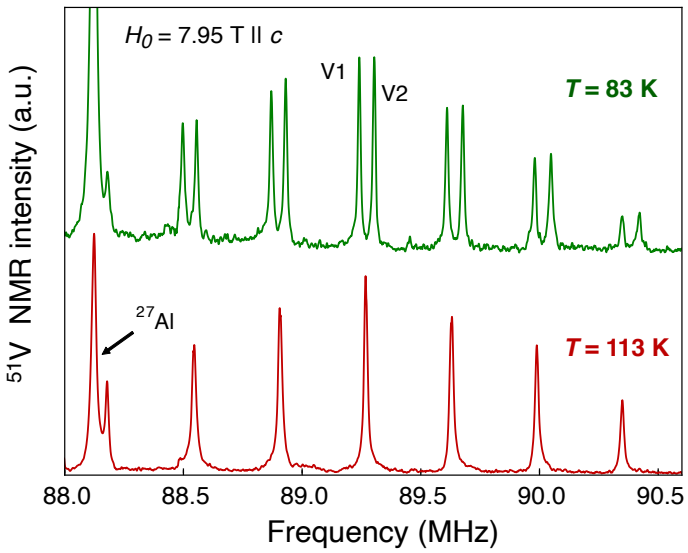

FIG. 1: Temperature dependence of the ^{51}V NMR spectra above and below $T_{\rm CDW}$, with the external magnetic field applied along the c axis. The peak around 88.3 MHz is from the ^{27}Al in the sample holder.

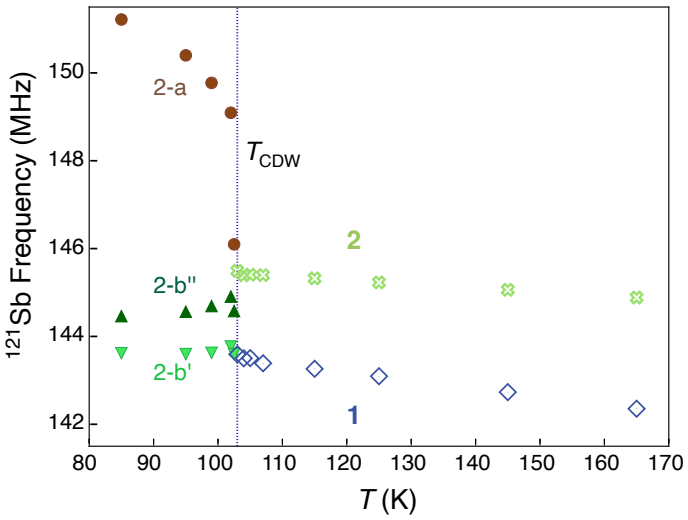

FIG. 2: Temperature dependence of the quadrupolar frequencies of ^{121}Sb for $5/2 \rightarrow 3/2$ NQR transition. The ^{121} sites are labeled in the figure. The sites 1-a and 1-b below the CDW are not present here because their NMR peaks are below the detection threshold in standard measuring conditions. They are recovered in exceptionally high statistic measurements (see Fig.2 main text).

III. SUPPLEMENTARY NOTES

A. ^{51}V NMR Spectra

Supplementary Figure 1 shows the spectra of ^{51}V with an external magnetic field H_0 = 7.95 T // c axis. When an external magnetic field H_0 is applied to a system of nuclei with nuclear spin $I > 1/2$[13,14], the total Hamiltonian of the system is:

$$\mathcal{H} = \mathcal{H}_0 + \mathcal{H}_Q = -\gamma\hbar \boldsymbol{I} \cdot \mu_0 \boldsymbol{H}(1+K) + \frac{e^2qQ}{4I(2I-1)}[(3I_z^2 - \boldsymbol{I}^2) + \frac{1}{2}\eta\left(I_+^2 + I_-^2\right)] \quad (1)$$

where K is the total Knight shift, $eq = V_{ZZ} = \frac{\partial V^2}{\partial Z^2}$ is the principal component of the electric field gradient (EFG) tensor along the principle axis system (PAS) and V is the electric potential, Q is the nuclear quadrupole moment, and η = $|V_{XX}$ - $V_{YY}|/|V_{ZZ}|$ is the asymmetry parameter of the EFG. ^{51}V has I = 7/2, indeed seven NMR peaks are shown above T_{CDW} = 103 K. Below T_{CDW}, two sets of new peaks arise, a proof of the CDW transition and results in the formation of two different vanadium sublattices, namely V1 and V2. The two vanadium sites have the same multiplicity, corresponding to the same area in the NMR spectra as in Supplementary Figure 1.

B. ^{121}Sb NQR spectra and quadrupolar frequency

NQR measurements on ^{121}Sb have been performed in zero-field (ZF) mode. In Supplementary Figure 2. the temperature behavior of 121 Sb quadrupolar frequencies is shown, for 5/2 → 3/2 NQR transition. Below T_{CDW}, only the 3 Sb2 sites are shown, which correspond to the 3 most intense peaks in the main text. Sb1 sites below T_{CDW} are not shown since they can only be seen with very high statistics, and therefore we could not observe their temperature dependence. In the main text, the selected 121 Sb NQR spectra above and below T_{CDW} are shown. Above T_{CDW} the two Sb sites, namely Sb1 and Sb2, have an intensity ratio of 1:4, in agreement with the multiplicity of the two sites. Below T_{CDW}, the CDW transition induces the formation of different sublattices for ^{121}Sb nuclei, as for ^{51}V and ^{87}Rb. Regarding the quadrupolar interactions of ^{121}Sb nuclei, we extracted the quadrupolar frequencies ν_Q from the experimental NQR spectra, considering the ^{121}Sb nuclear spin I = 5/2, and we compared them with the ones extracted from DFT calculations using the relation (valid for $\eta \leq 0.1$)[13,15]:

$$\nu_Q^{3/2\to1/2} = \frac{3eQV_{zz}}{20h}\left(1 + \frac{59}{54}\eta^2\right) \qquad \nu_Q^{5/2\to3/2} = \frac{3eQV_{zz}}{10h}\left(1 - \frac{11}{54}\eta^2\right) \quad (2)$$

where 3/2 → 1/2 and 5/2 → 3/2 represent the first and second NQR transitions for I = 5/2 nuclei, respectively. In the formula, Q is the quadrupole moment of the nucleus, V_{zz} the principal

component of the EFG tensor in the Principal Axis System (PAS), I the nuclear spin, and η the asymmetry parameter of the EFG tensor in the PAS notation. It can be seen that for $\eta = 0$, the $5/2 \rightarrow 3/2$ NQR transition frequency is exactly twice the one of $3/2 \rightarrow 1/2$ transition.

---

[1] B. R. Ortiz, S. M. L. Teicher, Y. Hu, J. L. Zuo, P. M. Sarte, E. C. Schueller, A. M. M. Abeykoon, M. J. Krogstad, S. Rosenkranz, R. Osborn, et al., Phys. Rev. Lett. **125**, 247002 (2020), URL https://link.aps.org/doi/10.1103/PhysRevLett.125.247002.

[2] Q. Yin, Z. Tu, C. Gong, Y. Fu, S. Yan, and H. Lei, Chinese Physics Letters **38**, 037403 (2021), ISSN 1741-3540, URL http://dx.doi.org/10.1088/0256-307X/38/3/037403.

[3] G. Allodi, A. Banderini, R. D. Renzi, and C. Vignali, Review of Scientific Instruments **76**, 083911 (2005), URL https://doi.org/10.1063/1.2009868.

[4] E. L. Hahn, Phys. Rev. **80**, 580 (1950), URL https://link.aps.org/doi/10.1103/PhysRev.80.580.

[5] D. M. S. Bagguley, *Pulsed Magnetic Resonance - NMR, ESR, and Optics: A Recognition of E. L. Hahn.* (Oxford University Press, 1992).

[6] W. G. Clark, M. E. Hanson, and F. Lefloch, Review of Scientific Instruments **66** (1995), URL https://aip.scitation.org/doi/citedby/10.1063/1.1145643.

[7] *Elk code v8.3.25*, URL elk.sf.net.

[8] M. Methfessel and A. T. Paxton, Phys. Rev. B **40**, 3616 (1989), URL https://link.aps.org/doi/10.1103/PhysRevB.40.3616.

[9] J. P. Perdew, K. Burke, and M. Ernzerhof, Phys. Rev. Lett. **77**, 3865 (1996), URL https://link.aps.org/doi/10.1103/PhysRevLett.77.3865.

[10] H. J. Monkhorst and J. D. Pack, Phys. Rev. B **13**, 5188 (1976), URL https://link.aps.org/doi/10.1103/PhysRevB.13.5188.

[11] J. D. Pack and H. J. Monkhorst, Phys. Rev. B **16**, 1748 (1977), URL https://link.aps.org/doi/10.1103/PhysRevB.16.1748.

[12] H. Tan, Y. Liu, Z. Wang, and B. Yan, Phys. Rev. Lett. **127**, 046401 (2021), URL https://link.aps.org/doi/10.1103/PhysRevLett.127.046401.

[13] A. Abragam, *The Principles of Nuclear Magnetism* (Oxford University Press, 1983).

[14] R. E. Wasylishen, *NMR Of Quadrupolar Nuclei In Solid Materials* (John Wiley and Sons, 2012).

[15] T. P. Das and E. L. Hahn, *Nuclear Quadrupole Resonance Spectroscopy* (American Institute of Physics, 1959).